Jpn. J. Appl. Phys. Vol. 40 (2001) pp. L 528–L 531
Part 2, No. 5B, 15 May 2001

Striation Mechanism and Triggered Striation in Dielectric Microdischarge Plasma

Jae Koo LEE*, Sheikh DASTGEER, Chae Hwa SHON, Min Sup HUR, Hyun Chul KIM and Suwon CHO[1]

Department of Electrical Engineering, Pohang University of Science and Technology, Pohang 790-784, S. Korea
[1]*Physics Department, Kyonggi University, Suwon 440-760, S. Korea*

(Received January 25, 2001; accepted for publication March 21, 2001)

The striation mechanism of dielectric microdischarges, as in many plasma devices, is extensively explored by collisional kinetic and fluid simulations. Striation in a typical dielectric microdischarge device predominantly occurs near the anode region and is basically governed by the ionization-dominated α-processes, wherein surface and space charges collectively dictate the phenomenon in a complex manner. A novel type of striation has been investigated by us near the cathode region, which is dominated by γ-processes and is driven by the secondary-electron emission mechanism.

KEYWORDS: striation, plasma discharge, plasma display panels, ionization, low temperature

Striation is well known in positive-column and ionospheric plasma systems, and is believed to be associated with the wave-related mechanism. Recently, there has been considerable interest in this phenomenon, in particular, related to dielectric microdischarge plasma systems.[1–3] Such systems deal with the discharge processes which occur on the spatial length scales ranging from sub-millimeter to millimeter. The most eminent example is the plasma display panel (PDP),[4,5] which has been attracting much attention recently because of its potential application in next-generation high definition display devices. Recently, it was observed in experiments[6,7] that during the evolution of discharge in a coplanar PDP, several bunches of localized discharges follow the striation process. The formation of striation in a negative-glow discharge (such as PDP), however, leads to several questions. For example, what is the actual self-consistent mechanism behind the onset and sustainment of the striation process, and is it possible that striation occurs near the cathode region? These issues are primarily concerned with the understanding of the discharge mechanism and still remain relatively unexplored. It is thus imperative to study the striation phenomenon in order to understand the discharge evolution in a microdischarge system.

An adequate understanding of striation could additionally contribute to the understanding of the striation in a positive-column[1] and in a dielectric barrier discharge, which have long been known of and which are widely believed to be primarily engendered by ion acoustic waves. The PDP discharge characteristics are basically different from the positive-column discharges. In this study, our prime endeavour is therefore to explore the striation phenomenon in a dielectric microdischarge, with a mechanism different from that involving the usual ion acoustic wave. We mainly concentrate here upon understanding the basic mechanism that governs this phenomenon. Our investigations, based on kinetic as well as fluid simulations, clearly demonstrate the striation phenomenon in PDP and also confirm the governing mechanism behind it. We further emphasize as well as provide several pieces of evidence, for the first time, that striation can occur near the cathode region in addition to the anode region. Such a novel kind of striation appears relatively weak as compared to the anode-side striation. However, it can be made (or triggered) as distinguishable as the anode-side striation by means of adequate tailoring of the dielectric constants and the secondary electron emission characteristics of the material near the cathode-side region.

The PDP geometry, considered in all our simulations, consists of two electrodes aligned in the same upper plate.[8,9] These electrodes are covered with MgO dielectric material, which is capable of emitting secondary electrons when energetic ions hit it. The lower address electrode is covered with phosphor dielectric. The length and width are 1260 μm and 210 μm, respectively. The gap between the two coplanar electrodes is 60 μm and the length of each electrode is 400 μm. The width and dielectric constant of the dielectric materials of the upper and lower sides are, respectively, 45 μm, 12, and 40 μm, 10. The applied voltages on the top-left, top-right and bottom electrodes are 300, 0, 150 V, respectively. We have carried out simulations for three different gas pressures, namely, 100, 200 and 500 Torr. The neutral gas composition is 96% Ne and 4% Xe. We use object-oriented particle-in-cell (OOPIC)[10] and fluid 2-dimensional PDP (FL2P)[8,9] codes for the purpose of kinetic and fluid simulations, respectively. The kinetic code is based upon the first-principles calculation (Newtonian equations), while the fluid code uses fluid continuity equations (for electron, ions, and excited species) along with drift-diffusion approximation. It is noteworthy that the phenomenon of striation using simulation has not been reported previously.[5,11–14]

The time development of striations, as observed in our kinetic simulation, is shown in Figs. 1(a)–1(d). The highly nonuniform distribution of plasma density along the length of the anode electrode is clearly evident. Although not presented in this paper, it was observed that the striation is more predominant in the high-pressure regime. Thus, we observed a relatively large number of plasma bunches as the pressure of the neutral gas was increased. Similarly, these bunches are distinctly separated from each other when the pressure is relatively high. Our results indeed show qualitatively similar traits to those observed in experiments.[6,7]

We now describe the self-consistent mechanism, based on various simulation diagnostics, which explains the onset and sustainment of the striation phenomenon. To begin, there exists a large electric field between the two electrodes, which ignites the nearby discharge by creating electron-ion plasma. The discharge then moves toward the cathode side. It remains there as a main bunch until the discharge-evolution in the anode-side is terminated. The corresponding time developments of potential and electron density profiles are shown in Fig. 2. These observations are made before and after the

*E-mail address: jkl@postech.ac.kr

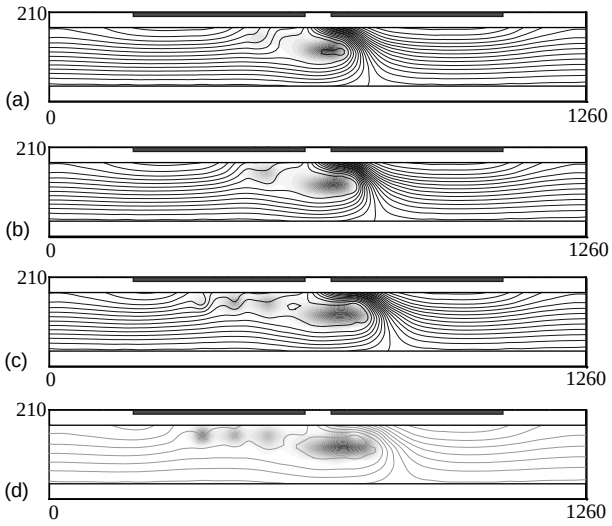

Fig. 1. Electron density (dark spots) along with electric potential contours (solid lines) are displayed at pressure 500 Torr for (a) $t = 101.252$ ns, (b) $t = 128.838$ ns, and (c) $t = 147.738$ ns. Striation near the anode side is clearly visible. The cathode-side striation begins to form at a later stage as shown in (c). (d) is the same figure as (c) except that the image contour level is slightly changed for a clearer image of the cathode-side striation.

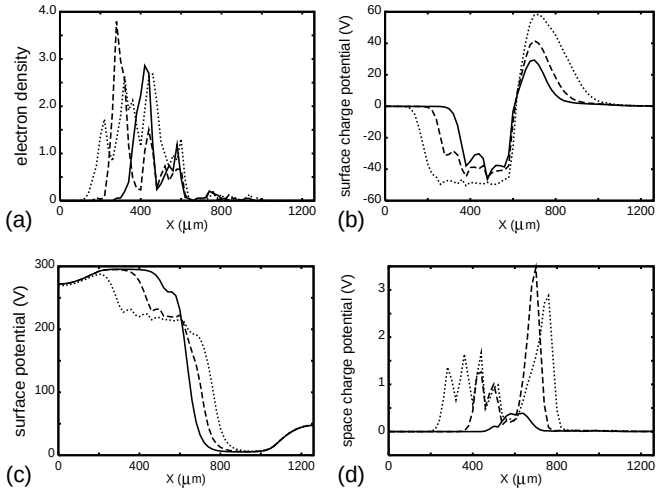

Fig. 2. Various profiles from the kinetic simulation for 500 Torr. (a) corresponds to the line profile of the surface electron density [in the unit of 10^{17}], (b) the total surface charge potential, (c) the surface potential, and (d) the total space charge potential at 10 μm below the front-dielectric, at various times. Solid, dashed and dotted lines belong to the initial ($t = 101.252$ ns), the intermediate ($t = 128.838$ ns) and later ($t = 147.738$ ns) times.

electron density number reaches its peak value. Electrons in the main bunch are pulled apart to the anode side by the high electric field between the anode and the cathode. These electrons then accumulate near the anode (behaving as surface charges), thereby reducing the applied voltage (flattening the voltage). Nevertheless, the potential difference between the flattened and applied potential is still higher than the ionization energy of the neutral gas. In this high electric field region, electrons gain sufficient energy to ionize the neutral gas and form another bunch (or peak). Then, the second bunch creates another flat potential region. This process continues in a similar manner until the combination of applied and surface potential becomes low and flat in the local region. The spatial distribution of the potential acquires a well-like shape and is sufficient to confine and produce electron species in the space. The potential difference between the two consecutive bunches decreases as one proceeds along the inner to the outer edge of the anode. Near the outer edge, sufficient surface charges accumulate and flatten out the potential. Thereafter, the striation process is terminated. The surface charge density profile, consisting of several peaks, is shown in Fig. 2(b). As time advances, the surface charge structures follow the plasma density fluctuation in space. This means that the plasma particles respond self-consistently to the combined electric field of applied and surface charge potentials. As the surface charge profile changes with time, the space-charge potential follows [see Fig. 2]. The first flat potential region in the first observation time corresponds to the first appearing plasma bulk region. It thus seems clear that surface and space charges influence each other in a complex fashion and thus cause striation phenomena.

The experimental results of vacuum ultraviolet (VUV) emission spectrum[6] compare qualitatively well with the time development of excited Xe density observed in the simulation. As a quantitative estimation, we measure the speeds of the electron and the ion bunch formation (or peak development) and compare them with the experimental results.[6,7] The development speeds of the cathode-side and the anode-side density fronts in the simulation are found to be about 1.35 km/s and 7.8 km/s, respectively, which are in fairly good agreement with the experimentally observed speeds of 2.0 km/s at the cathode side and 7.5 km/s at the anode side. Although the conditions in the experiment and the simulation are slightly different, the orders of magnitude reveal an excellent match between them.

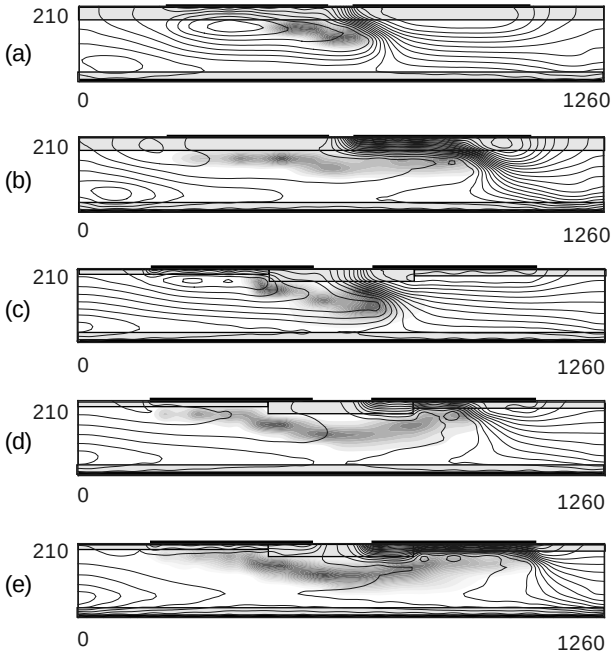

Fig. 3. Conventional striation at 500 Torr, with uniform dielectric, is shown for (a) $t = 169.0$ ns and (b) $t = 262.0$ ns. The triggered striation due to the three pieces of the dielectric is shown for (c) $t = 264.0$ ns, (d) $t = 325.0$ ns, and (e) $t = 371.0$ ns. Dark spots and solid contour lines indicate the excited Xe density and the potential, respectively. Fluid code results at various time sequences are plotted. Striation on the cathode side appears distinguishably in (c), (d) and (e) due to dielectric constant tailoring.

Striation phenomenon is also observed in the simulation of fluid equations [eqs. (1)–(5)]. This is shown in Figs. 3(a) and 3(b). However, it is less clear compared with that in the kinetic simulation. In the fluid treatment, electron bunches are susceptible to rapid smearing. The basic reason for this could be the fact that the fluid code uses the drift-diffusion and the local-field approximations.[8,9,11–14)]

$$\frac{\partial n_e}{\partial t} + \nabla \cdot \Gamma_e = R_i - \alpha n_e n_p, \tag{1}$$

$$\frac{\partial n_p}{\partial t} + \nabla \cdot \Gamma_p = R_i - \alpha n_e n_p, \tag{2}$$

$$\nabla \cdot (\epsilon \nabla V) = -e(n_p - n_e), \tag{3}$$

$$\Gamma_e = -D_e \nabla n_e - n_e \mu_e E, \tag{4}$$

$$\Gamma_p = -D_p \nabla n_p + n_p \mu_p E, \tag{5}$$

where $n_{p,e}$, $D_{p,e}$, $\mu_{p,e}$ are the density, diffusion and mobility of electron (ion), respectively. ϵ, R_i, α, are the permittivity, ionization rate coefficient, and recombination efficient, respectively. In the fluid treatment, the localization of electric field is not sufficiently effective enough to maintain striation bunches distinctly for a longer time. However, the mechanism of concatenation occurrence of striation bunches in fluid treatment is the same as that described earlier. As the number of spatial bunches increases with time, the time evolution of the density of electrons, ions or excited species shows spikes. Thus, spatial striation patterns are associated with temporal spikes of densities.

It is interesting to report here that striation may also occur near the cathode region. Such striation has not been predicted or reported previously. However, it is clearly evident from our simulation results [see Fig. 1(d)] that striation does occur near the cathode region. This type of novel striation is markedly different from the conventional anode-side striation, and is governed by the secondary-electron emission (SEE) process. During this process, the energetic ion flux to the boundary dielectric gives rise to a population of electrons, which then form a striation. Such a striation is therefore governed by γ-processes.[2)] Slow ion motion is involved in this type of striation, therefore, it occurs at relatively slow time scales and is imperceptible when compared with the anode-side striation in Fig. 1(d). Only two striation bunches at the cathode side are observed but the number of these cathode-side striations will likely increase with time.

Nevertheless, such striation can be made discernible by adequate tailoring of dielectric constants or/and the secondary electron coefficient of the dielectric material. For example, a triggered striation by three-piece dielectrics, as shown in Figs. 3(c)–3(e), possesses a similar pattern to that of the untriggered (or conventional) one. Similarly, the triggered striation by nine-piece dielectrics, as shown in Figs. 4(a) and 4(b) exhibits striation patterns at both the electrodes. These striation patterns appear more clearly than those in a typical uniform dielectric as in Figs. 3(a) and 3(b). Another type of triggered striation [as in Figs. 4(c)–4(e)] shows a strikingly different pattern particularly in the plasma region near the cathode side. Due to the tailored SEE coefficient (SEEC) with a much lower value at the two locations slightly away from the middle of the upper dielectric, the plasma generation at the anode side via ionization is the same as before, as shown in Fig. 3(a)

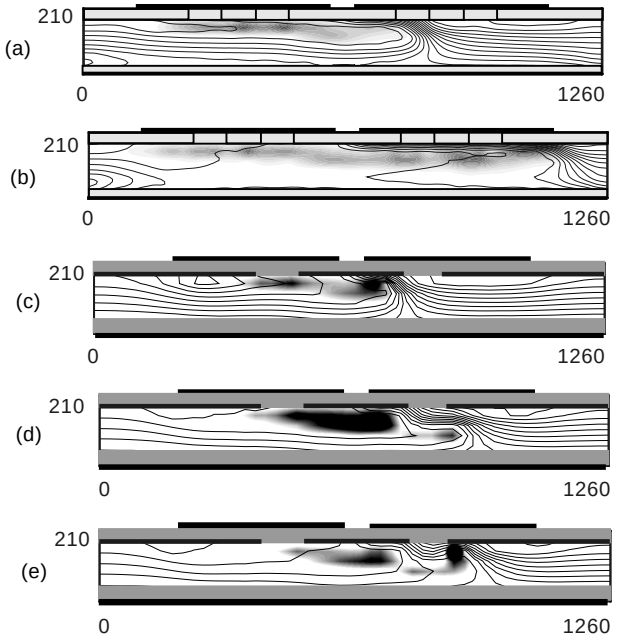

Fig. 4. The triggered striation by means of nine pieces of the dielectric (where the dielectric constants from left are 24, 2, 18, 2, 12, 2, 18, 2, 24) is shown for (a) $t = 170.5$ ns and (b) $t = 284.1$ ns. The pressure is 500 Torr. Similar quantities (as in Fig. 3) are shown. The triggered striation due to γ-tailoring is shown for (c) $t = 150.0$ ns, (d) $t = 290.0$ ns and (e) $t = 360.0$ ns. Thick lines on the dielectric refer to the presence of SEEC, where plasma bunches appear pronounced. The empty region indicates the absence of SEEC, where electron density is extremely low. Striation near the cathode side is conspicuous.

(namely, it is governed by the space electric field) but that via secondary electrons are controlled by this SEEC tailoring. Resultantly, not much SEE is expected near the cathode side and the overall plasma density profile is significantly altered [see Fig. 4(e)]. These results confirm the dominance of the γ-mode discharge process[2)] in the cathode-side striation.

In conclusion, we have comprehensively explored the phenomenon of striation in a microdischarge system (as in coplanar AC PDP) using a variety of numerical experiments. The origin of striations is due to concomitant action and the influence of surface and space charges, which alter the local electric potential, density and electric field profiles and form coherent bunches. The striation mechanism, as confirmed by our simulation, is clearly associated with the dielectric charge accumulation affecting the space charge and the potential distribution, but not specifically with any wave phenomenon. Striation near the anode side is more prominent than that near the cathode side. Specific types of striation can be triggered at the cathode as well as at the anode locations by specific dielectric constants or SEEC. For the latter type of triggered striation, there is an ionization-dominated α-mode in the plasma-sheath region at the anode side, and a SEE-dominated γ-mode in that at the cathode side.

The authors would like to thank Professor K. Tachibana for helpful discussion and suggestions. The present study was supported by LG Electronics and the Ministry of Education of Korea through its BK21 program.

1) M. Turner: *IEEE Int. Conf. Plasma Science, New Orleans, 2000*, p. 163.
2) Y. P. Raizer, M. N. Shneider and N. A. Yatsenko: *Radio-Frequency Ca-*

pacitive Discharges (CRC Press, 1995).
3) A. V. Gurevich, K. P. Zybin and A. V. Lukyanov: Phys. Rev. Lett. **75** (1995) 2622.
4) M. A. Lieberman: *Advance Tech. Based on Wave & Beam Generated Plasmas*, eds. H. Schlueter and A. Shivarova (Kluwer, 1999) pp. 1–22.
5) J. K. Lee and J. P. Verboncouer: *Lectures in Plasma Science & Plasma Technology*, eds. S. Pfau, M. Schmidt, R. Hippler and K. H. Schoenbach (Wiley-VCH, 2001).
6) T. Yoshioka, A. Okigawa, L. Tessier and K. Toki: *Proc. Sixth Int. Display Workshop '99, Sendai, 1999*, p. 603.
7) G. Cho, E. Choi, Y. Kim, D. Kim, H. Uhm, Y. Joo, J. Han, M. Kim and J. Kim: J. Appl. Phys. **87** (2000) 4113.
8) Y. K. Shin, C. H. Shon, W. Kim and J. K. Lee: IEEE Trans. Plasma Sci. **27** (1999) 1366.
9) Y. K. Shin, J. K. Lee, C. H. Shon and W. Kim: Jpn. J. Appl. Phys. **38** (1999) L174.
10) J. P. Verboncoeur, A. B. Langdon and N. T. Gladd: Comput. Phys. Commun. **87** (1995) 199.
11) S. Rauf and M. J. Kushner: J. Appl. Phys. **85** (1999) 3460.
12) C. Punset, J. P. Boeuf and L. C. Pitchford: J. Appl. Phys. **83** (1998) 1884.
13) R. B. Campbell, R. Veerasingam and R. T. McGrath: IEEE Trans. Plasma Sci. **27** (1999) 1366.
14) V. P. Nagorny, P. J. Drallos and W. Williamson, Jr.: J. Appl. Phys. **77** (1995) 3645.